

# Interface dipole enhancement effect and enhanced Rayleigh scattering

Wenyun Wu<sup>1,§</sup>, Jingying Yue<sup>1,§</sup>, Dongqi Li<sup>1</sup>, Xiaoyang Lin<sup>1</sup>, Fangqiang Zhu<sup>2</sup>, Xue Yin<sup>3</sup>, Jun Zhu<sup>3</sup>, Xingcan Dai<sup>1</sup> (✉), Peng Liu<sup>1</sup>, Yang Wei<sup>1</sup>, Jiaping Wang<sup>1</sup>, Haitao Yang<sup>1</sup>, Lina Zhang<sup>1</sup>, Qunqing Li<sup>1</sup>, Shoushan Fan<sup>1</sup>, and Kaili Jiang<sup>1,4</sup> (✉)

<sup>1</sup> State Key Laboratory of Low-Dimensional Quantum Physics, Department of Physics & Tsinghua-Foxconn Nanotechnology Research Center, Tsinghua University, Beijing 100084, China

<sup>2</sup> Department of Physics, Indiana University-Purdue University Indianapolis, Indianapolis, Indiana, USA

<sup>3</sup> State Key Laboratory of Precision Measurement Technology and Instruments, Department of Precision Instruments, Tsinghua University, Beijing 100084, China

<sup>4</sup> Collaborative Innovation Center of Quantum Matter, Beijing 100084, China

<sup>§</sup> These authors contributed equally to this work.

**Received:** 7 November 2014

**Revised:** 4 December 2014

**Accepted:** 7 December 2014

© Tsinghua University Press and Springer-Verlag Berlin Heidelberg 2014

## KEYWORDS

interface dipole enhancement, dielectric sphere, near field, nanomaterials, carbon nanotubes, Rayleigh scattering

## ABSTRACT

The optical effect of a nanometer or sub-nanometer interfacial layer of condensed molecules surrounding individual nanomaterials such as single-walled carbon nanotubes (SWCNTs) has been studied theoretically and experimentally. This interfacial layer, when illuminated by light, behaves as an optical dipole lattice and contributes an instantaneous near field which enhances the local field on neighboring atoms, molecules, or nanomaterials, which in turn may lead to enhanced Rayleigh scattering, Raman scattering, and fluorescence. The theory of this interface dipole enhanced effect (IDEE) predicts that a smaller distance between the nanomaterials and the plane of the interfacial layer, or a larger ratio of the dielectric constants of the interfacial layer to the surrounding medium, will result in a larger field enhancement factor. This prediction is further experimentally verified by several implementations of enhanced Rayleigh scattering of SWCNTs as well as *in situ* Rayleigh scattering of gradually charged SWCNTs. The interface dipole enhanced Rayleigh scattering not only enables true-color real-time imaging of nanomaterials, but also provides an effective means to peer into the subtle interfacial phenomena.

## 1 Introduction

Interfaces are subtle because of their nanoscale

dimension, but play many important roles in physical, chemical, and biological phenomena. For a nano-object immersed in a medium, the interface is more

Address correspondence to Xingcan Dai, XingcanDai@tsinghua.edu.cn; Kaili Jiang, JiangKL@tsinghua.edu.cn

important and interesting than that for a macro-object, because the dimensions of the nano-object are on the same order as the interface which may lead to strong mutual interactions.

For single-walled carbon nanotubes (SWCNTs), sub-nanometer shells of high refractive index form at the interface when SWCNTs are immersed in a liquid medium, such as water [1, 2]. Recently we discovered that the sub-nanometer shells on SWCNTs can greatly enhance the Rayleigh scattering of SWCNTs, which further enables true-color real-time imaging of SWCNTs under an optical microscope [3]. This enhancement effect is termed “interface dipole enhancement effect (IDEE)”, because the interfacial shell serves as an optical dipole lattice and contributes to an enhanced local field for the excitation of SWCNTs when illuminated by light.

In this report, we present a general theoretical treatment and experimental verification of IDEE. Perspectives on the consequences and applications of IDEE are also discussed.

## 2 General theory of the interface dipole enhancement effect (IDEE)

The goal of this theory is to investigate the optical effect of a nanometer or sub-nanometer interfacial layer of condensed molecules surrounding individual nanomaterials such as SWCNTs. The nanometer dimensions of both nanomaterials and the interfacial layers mean that the microscopic field rather than the macroscopic field should be calculated. On the other hand, the fact that the nanomaterials are much smaller than the wavelength of light justifies the static field approximation which greatly simplifies the calculations. Details are shown below.

In the following text, we will take SWCNTs as an example to discuss IDEE on nanomaterials. However, it is worth noting that the following discussion about IDEE is not restricted to SWCNTs, but is widely applicable to any nanomaterial whose size is smaller than the lattice spacing of optical dipole chains (See Sections 2.7 and 2.8).

### 2.1 Macroscopic field, microscopic (local) field, and near field

When the classical electrodynamics simulation is

carried out using the macroscopic parameters of a medium such as dielectric constant or index of refraction, the calculated field is a macroscopic quantity. It is well known that “the value of a macroscopic quantity at a point  $P$  is an average of the microscopic quantity over a region of dimensions  $r_0$  in the neighborhood of  $P$ , where  $r_0$  is large compared to the interparticle spacing  $a$ ” [4]. Considering the fact that a SWCNT is a nanomaterial with a thickness of only about one atom, we calculate the microscopic field (also termed “local field”) rather than the macroscopic field.

In the microscopic picture, the atoms or molecules of the surrounding medium are driven by a light field to oscillate as optical dipoles, resulting in secondary radiation (or scattering). Thus the microscopic field is the vector addition of the excitation light field and secondary radiation field of all the optical dipoles.

In a homogeneous medium, the secondary radiation field of all the optical dipoles cancels in all directions except the direction of propagation of the incident light [5]. For a homogeneous medium with negligible absorption, such as water or glycerol, the total field contributed by all the optical dipoles can also be simply described by a macroscopic quantity—index of refraction, according to the calculated field from an infinite sheet of oscillating dipoles [6, 7]. In this sense, the microscopic and macroscopic descriptions are equivalent.

However, when the distance between a SWCNT and the adjacent optical dipole lattice is smaller than the lattice spacing of the optical dipole lattices, the SWCNT will also feel the near field of the optical dipole lattice, which is not accessible in the macroscopic picture. In this case, the microscopic field felt by the SWCNT is the vector addition of the excitation light field, the far field contributed by all the optical dipoles, and the near field of the adjacent optical dipoles. The vector addition of the former two parts is equal to the macroscopic field in the condensed medium. The microscopic field felt by the SWCNT is therefore the vector addition of the macroscopic field and the near field of the adjacent optical dipoles.

Here we would like to stress that the near field of an optical dipole is different from the “near field” concept in optics which is defined relative to the

wavelength of the light. The near field of an optical dipole decays to zero within a distance which could range from angstrom to tens of nanometers depending on the size of the optical dipoles.

In the following discussions, we adopt the microscopic picture to calculate the near field of optical dipoles.

## 2.2 Static field approximation

To investigate the near field of optical dipoles, a static field approximation is adopted on the basis of the following considerations:

(1) The optical dipoles far away from a SWCNT contribute to the retarded far field, which can be well described by the index of refraction. Only the optical dipoles in the vicinity of a SWCNT contribute to the near field.

(2) The dimension of a SWCNT and the interface optical dipoles is much smaller than the visible wavelength, thus the optical dipoles in the vicinity of SWCNT oscillate simultaneously. The near field is therefore instantaneous rather than retarded.

The static field approximation greatly simplifies the calculations, as is shown later.

## 2.3 Dipole field of a dielectric sphere in vacuum

We start from the case of a dielectric sphere irradiated by incident light. When the diameter of the dielectric sphere is much smaller than the wavelength of the incident light, the static field approximation is justified. In the following discussions, we will omit the time varying part  $e^{i\omega t}$  and use the static field only.

Considering a dielectric sphere in a light field  $\vec{E}_0$ , each atom or ion or molecule (we will use “atom” only to represent the building blocks of the dielectrics) in the sphere is forced to oscillate in phase with the light field. The induced optical dipole of the atom is  $\vec{p}_0 = \alpha \epsilon_0 \vec{E}_{\text{local}}$ , in which  $\epsilon_0$  is the permittivity of the vacuum,  $\alpha$  (with the dimension  $L^3$ ) is the atomic polarizability at optical frequency [7], and  $\vec{E}_{\text{local}}$  is the local field at the position of the atom. Note that at optical frequencies, the polarizability can only be induced by the motion of electrons, which is quite different from the static polarizability induced by motions of both electrons and ions, and rotations of

polar molecules. In the following discussions, we are only concerned with optical frequency polarizability. As for the local field at the position of the atom, following the discussion with the help of an imaginary Lorentz cavity [8], we have  $\vec{E}_{\text{local}} = \vec{E}_0 + \vec{E}_1 + \vec{E}_2 + \vec{E}_3$ , in which  $\vec{E}_1$  is the depolarization field of the dielectric sphere,  $\vec{E}_2$  is the Lorentz cavity field, and  $\vec{E}_3$  is the field of atoms inside the cavity. For an isotropic medium or cubic lattice of crystals,  $\vec{E}_3$  is equal to 0. In addition, it is easy to show that  $\vec{E}_1 + \vec{E}_2 = 0$  for the dielectric sphere. We therefore have  $\vec{E}_{\text{local}} = \vec{E}_0$  and

$$\vec{p}_0 = \alpha \epsilon_0 \vec{E}_0 \quad (1)$$

These induced optical dipoles will excite secondary radiation, which is in phase with the light field  $\vec{E}_0$  within the vicinity of the dielectric spheres where the static field approximation is justified. Static field calculations indicate that the macroscopic field inside the sphere is uniform but weakened due to the depolarization field. The dipole field outside the sphere can be easily obtained by integrating the field of each dipole.

The electric potential at position  $\vec{r}$  outside the sphere is

$$\phi_D(\vec{r}) = \frac{1}{4\pi\epsilon_0} \cdot \sum_i \frac{\vec{p}_0 \cdot (\vec{r} - \vec{r}'_i)}{|\vec{r} - \vec{r}'_i|^3} \quad (2)$$

in which  $\vec{r}'_i$  denotes the position of the  $i$ th optical dipole. Under the condition of continuous approximation, the expression of electric potential  $\phi_D(\vec{r})$  (Eq. (2)) becomes an integral over the volume inside the sphere

$$\phi_D(\vec{r}) = \frac{1}{4\pi\epsilon_0} \cdot \iiint_V \frac{\vec{P} \cdot (\vec{r} - \vec{r}')}{|\vec{r} - \vec{r}'|^3} d^3r' \quad (3)$$

in which the polarization  $\vec{P}$  is defined as the mean dipole moment density  $\vec{P} = \frac{M\vec{p}_0}{V}$ .  $M$  is the total number of optical dipoles inside the sphere and  $V$  is the volume of the dielectric sphere. Then the electric potential  $\phi_D(\vec{r})$  is given by

$$\phi_D(\vec{r}) = \frac{1}{4\pi\epsilon_0} \cdot \frac{M\vec{p}_0 \cdot \vec{r}}{|\vec{r}|^3} \quad (4)$$

Equation (4) indicates that the field outside the sphere is equivalent to the field of a huge dipole centered at the sphere with the dipole moment equal to the sum of all the dipoles inside the sphere (as shown in Fig. 1). An equivalent dipole  $\vec{p}$  is used for convenience

$$\vec{p} = M\vec{p}_0 \quad (5)$$

Now we can calculate the dipole field outside the dielectric sphere simply using the following equation

$$\vec{E}_D(\vec{r}) = \frac{1}{4\pi\epsilon_0} \cdot \frac{3(\hat{r} \cdot \vec{p})\hat{r} - \vec{p}}{|\vec{r}|^3} \quad (6)$$

Therefore, the dipole field at the surface of the dielectric sphere is

$$\vec{E}_D(r=R) = \frac{N}{3\epsilon_0} \cdot [3(\hat{r} \cdot \vec{p}_0)\hat{r} - \vec{p}_0] \quad (7)$$

in which  $N = \frac{M}{V}$  is the number density of the dipoles in the dielectric sphere and  $\hat{r}$  is the unit vector. An interesting consequence is that the dipole field at the surface of the dielectric sphere is a constant regardless of the diameter of the sphere.

According to Eqs. (1) and (7), the dipole field at the poles (position S in Fig. 1) is

$$\vec{E}_D(\vec{r}_S) = \frac{1}{4\pi\epsilon_0} \cdot \frac{2\vec{p}}{|\vec{r}|^3} = \frac{2N\vec{p}_0}{3\epsilon_0} = \frac{2}{3}N\alpha\vec{E}_0 \quad (8)$$

The total field at position S is

$$\vec{E}(\vec{r}_S) = \vec{E}_0 + \vec{E}_D(\vec{r}_S) = \vec{E}_0 + \frac{2}{3}N\alpha\vec{E}_0 = \left(1 + \frac{2}{3}N\alpha\right)\vec{E}_0 \quad (9)$$

The dipole field at the equator (position T in Fig. 1) is

$$\vec{E}_D(\vec{r}_T) = \frac{-1}{4\pi\epsilon_0} \cdot \frac{\vec{p}}{|\vec{r}|^3} = \frac{-N\vec{p}_0}{3\epsilon_0} = -\frac{1}{3}N\alpha\vec{E}_0 \quad (10)$$

The total field at position T is

$$\vec{E}(\vec{r}_T) = \vec{E}_0 + \vec{E}_D(\vec{r}_T) = \vec{E}_0 - \frac{1}{3}N\alpha\vec{E}_0 = \left(1 - \frac{1}{3}N\alpha\right)\vec{E}_0 \quad (11)$$

It is clear that the fields are enhanced at both poles, but weakened at the equator of the sphere. Thus the presence of the dielectric sphere leads to distortion of the light field, leaving some regions with enhanced field and some with weakened field. If atoms, molecules, or nanomaterials fall into the enhanced region, they will feel an enhanced field, which may lead to enhanced Raman scattering, enhanced fluorescence, or enhanced Rayleigh scattering. This enhancement effect is named the interface dipole enhancement effect (IDEE).

To evaluate the enhancement effect, the enhancement factor is introduced, which is defined as the ratio of

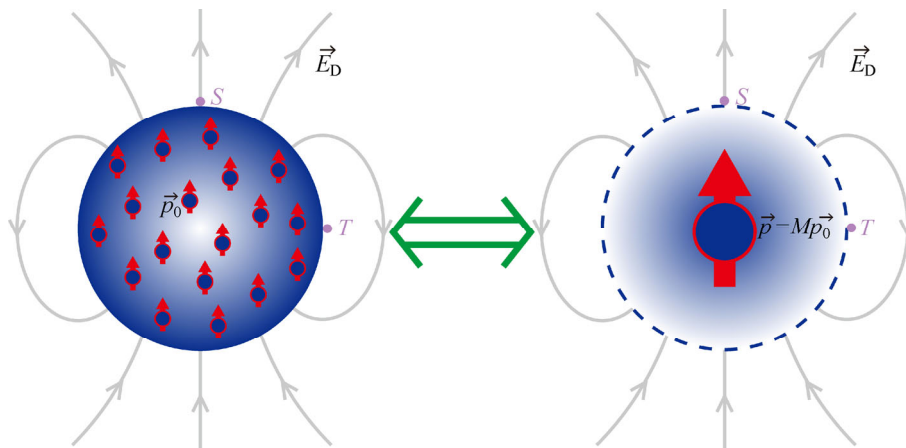


**Figure 1** Dipole field of a dielectric sphere. When illuminated by light, the atoms inside the dielectric sphere are polarized as optical dipoles and emit secondary radiation. The radiation field of the optical dipoles in the space apart from the interior of the sphere is equivalent to the radiation field of a single dipole centered in the sphere whose dipole moment is the sum of all the optical dipoles.

the intensity of the total light field  $\vec{E}$  and the excitation light field  $\vec{E}_0$ , i.e.

$$F = |\vec{E}|^2 / |\vec{E}_0|^2 \quad (12)$$

According to Eqs. (9) and (12), the enhancement factor at the poles (position S in Fig. 1) is

$$F(\vec{r}_s) = |\vec{E}(\vec{r}_s)|^2 / |\vec{E}_0|^2 = \left(1 + \frac{2}{3}N\alpha\right)^2 \quad (13)$$

For practical applications, it is more convenient to use a macroscopic parameter such as the dielectric constant  $\epsilon_r$ , or refractive index  $n$ . According to the Clausius–Mossotti relation [7],  $\epsilon_r - 1 = \frac{N\alpha}{1 - (N\alpha/3)}$ , the enhancement factor can be rewritten as

$$F(\vec{r}_s) = |\vec{E}(\vec{r}_s)|^2 / |\vec{E}_0|^2 = \left(\frac{3\epsilon_r}{\epsilon_r + 2}\right)^2 \quad (14)$$

Since  $\epsilon_r = n^2$ , it can also be expressed as

$$F(\vec{r}_s) = |\vec{E}(\vec{r}_s)|^2 / |\vec{E}_0|^2 = \left(\frac{3n^2}{n^2 + 2}\right)^2 \quad (15)$$

It is interesting that the field enhancement factor at the poles is a constant  $\left(\frac{3\epsilon_r}{\epsilon_r + 2}\right)^2$  regardless of the diameter of the sphere, provided that the static field approximation is justified.

In the aforementioned calculation of the dipole field outside the sphere, we do not consider the near field due to the optical dipoles on the surface of the sphere, which only exists in the region above the surface within one lattice distance of the dielectrics. In the following discussions about the field of dielectric spheres, this near field is neglected because it plays a negligible role. Furthermore, since the field outside the dielectric is independent of the diameter of the sphere, finite difference time domain (FDTD) simulation can be applied to retrieve the field pattern, as is shown below.

## 2.4 Hot spots generated by multiple dielectric spheres

The field intensity pattern of a dielectric sphere

irradiated by a 600 nm monochromatic light was simulated by the FDTD method. The result is shown in Fig. 2(a). It is clear that the dipole field only changes the light field in the vicinity of these spheres, showing the short range nature of the near field of the optical dipoles. As expected, the macroscopic field inside the dielectric sphere is a uniform field with intensity lower than excitation light intensity due to the depolarization field. The field intensity distribution outside the sphere agrees well with our microscopic calculation. It is enhanced at the poles and weakened at the equator.

The enhancement effect by dielectric spheres is very similar to the surface plasmon enhancement effect of metallic spheres. In fact, a metallic sphere irradiated by incident light can also be regarded as an optical dipole centered at the sphere. In this sense, the enhancement effect by metallic spheres is also an interface dipole enhancement effect with  $\epsilon_r \rightarrow -\infty$ , thus a larger enhancement factor. Details will be discussed in Section 2.5.

Note that the combinations of multiple dielectric spheres can also create “hot-spots” just like for metallic spheres, as shown in Figs. 2(b)–2(d), which can be used to enhance signals of Raman spectroscopy, fluorescence, and Rayleigh scattering.

For the hot-spot between two adjacent spheres shown in Fig. 2(b), the enhancement factor can be approximately derived from Eqs. (14) and (15) by applying the superposition principle

$$F \approx \left(\frac{5\epsilon_r - 2}{\epsilon_r + 2}\right)^2 = \left(\frac{5n^2 - 2}{n^2 + 2}\right)^2 \quad (16)$$

For the hot-spot of two adjacent water spheres ( $n = 1.33$ ), the enhancement factor is estimated to be around 3.3. For that of glycerol ( $n = 1.47$ ), the enhancement factor is around 4.5. Therefore the IDEE will lead to a  $4.5\times$  increase in fluorescence signals, and a  $20\times$  increase in Raman signals if the sample is placed in the hot-spot between two adjacent glycerol spheres.

## 2.5 Dipole field of dielectric spheres in a medium

For dielectric spheres immersed in a medium with dielectric constant  $\epsilon_m$ , it is not easy to follow the

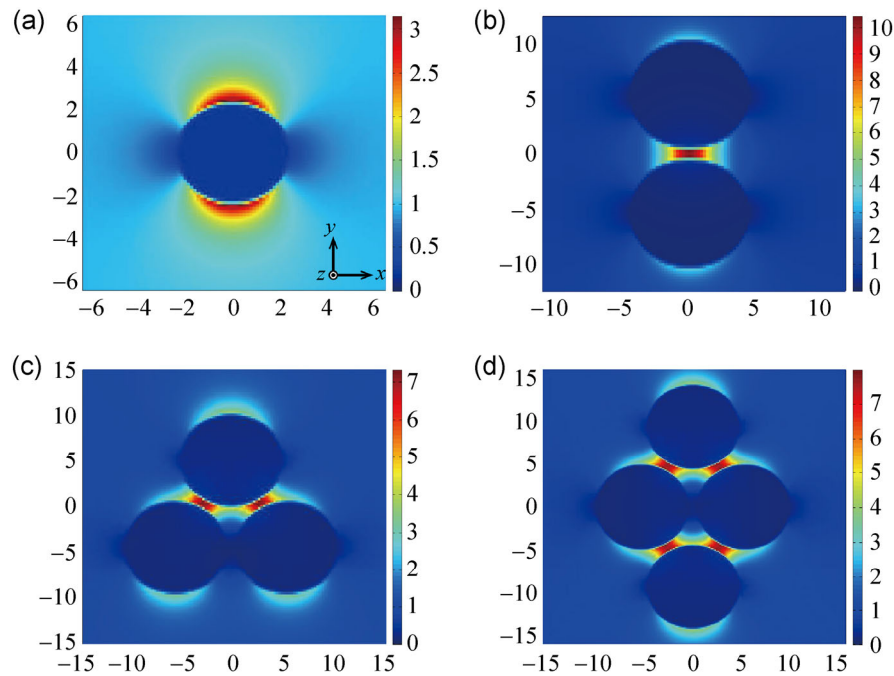


**Figure 2** Finite difference time domain simulations of the field intensity of dielectric spheres. The incident light which is polarized along the  $y$  axis propagates along the  $z$  axis and the field is calculated under illumination by monochromatic light with 600 nm wavelength. The axes take nanometer as unit. (a) The field intensity of a dielectric sphere and the fields at the two poles are enhanced, but weakened at the equator and inside the sphere. The diameter of the dielectric particle is 5 nm. (b)–(d) Hot-spots generated by multiple dielectric spheres. Because of the vertically polarized light, there are hot-spots between the two dielectric spheres which are separated along  $y$  direction. However, the field between the dielectric spheres separated along  $x$  direction is not enhanced. The diameter of all the nanoparticles is 10 nm.

method shown in Section 2.3. However, for an individual dielectric sphere immersed in a medium and irradiated by light, an analytical solution can be easily obtained by solving the Laplace equation [9, 10].

The macroscopic field inside a dielectric sphere with radius  $R$  is

$$\vec{E}(r < R) = \frac{3\epsilon_{\text{m}}}{\epsilon_{\text{r}} + 2\epsilon_{\text{m}}} \cdot \vec{E}_0 \tag{17}$$

The field outside the dielectric sphere is

$$\vec{E}(r > R) = \vec{E}_0 + \vec{E}_{\text{D}} \tag{18}$$

in which

$$\vec{E}_{\text{D}} = \frac{1}{4\pi\epsilon_0\epsilon_{\text{m}}} \cdot \frac{3(\hat{r} \cdot \vec{p})\hat{r} - \vec{p}}{|\vec{r}|^3} \tag{19}$$

$$\vec{p} = 4\pi R^3 \epsilon_0 \epsilon_{\text{m}} \cdot \frac{\epsilon_{\text{r}} - \epsilon_{\text{m}}}{\epsilon_{\text{r}} + 2\epsilon_{\text{m}}} \vec{E}_0 \tag{20}$$

Then the field enhancement factor at the poles is

$$F(\vec{r}_s) = |\vec{E}(\vec{r}_s)|^2 / |\vec{E}_0|^2 = \left( \frac{3\epsilon_{\text{r}}}{\epsilon_{\text{r}} + 2\epsilon_{\text{m}}} \right)^2 = \left( \frac{3n^2}{n^2 + 2n_{\text{m}}^2} \right)^2 \tag{21}$$

For the hot-spot between two adjacent dielectric spheres, the enhancement factor follows

$$F \approx \left( \frac{5\epsilon_{\text{r}} - 2\epsilon_{\text{m}}}{\epsilon_{\text{r}} + 2\epsilon_{\text{m}}} \right)^2 = \left( \frac{5n^2 - 2n_{\text{m}}^2}{n^2 + 2n_{\text{m}}^2} \right)^2 \tag{22}$$

The results in the medium shown in Eqs. (17)–(22) are more general than those in vacuum. Simply by substituting  $\epsilon_{\text{m}}$  and  $n_{\text{m}}$  with 1, the results in vacuum can be immediately retrieved (Eqs. (14)–(16)).

Another consequence is that when  $\epsilon_{\text{m}}$  is increased, the field enhancement factor is decreased. If  $\epsilon_{\text{m}} = \epsilon_{\text{r}}$ , the enhancement factor is equal to 1, indicating no change of the field. This is just the consequence of a perfect refractive index matching. When  $\epsilon_{\text{m}} > \epsilon_{\text{r}}$ ,

the enhancement factor is less than 1, implying a weakened field.

## 2.6 IDEE versus surface plasmon enhancement effect

A metal sphere with dimensions much smaller than the wavelength of light also behaves as an optical dipole when irradiated by light. In the case of a static field, the field inside the metal sphere is zero, implying an infinite dielectric constant. Thus the general formulae (Eqs. (17)–(22)) for the dielectric sphere can also be applied to metal spheres by imposing the condition of  $\epsilon_r \rightarrow -\infty$ , because the real part of the dielectric function of Drude electrons in a metal is negative, and approaches infinity at low frequencies [10].

The macroscopic field inside the metal sphere with radius  $R$  is

$$\vec{E}(r < R) = \lim_{\epsilon_r \rightarrow -\infty} \frac{3\epsilon_{\text{rm}}}{\epsilon_r + 2\epsilon_{\text{rm}}} \cdot \vec{E}_0 = 0 \quad (23)$$

The field outside the metal sphere is

$$\vec{E}(r > R) = \vec{E}_0 + \vec{E}_D \quad (24)$$

in which

$$\vec{E}_D = \frac{1}{4\pi\epsilon_0\epsilon_{\text{rm}}} \cdot \frac{3(\hat{r} \cdot \vec{p})\hat{r} - \vec{p}}{|\vec{r}|^3} \quad (25)$$

$$\vec{p} = \lim_{\epsilon_r \rightarrow -\infty} 4\pi R^3 \epsilon_0 \epsilon_{\text{rm}} \cdot \frac{\epsilon_r - \epsilon_{\text{rm}}}{\epsilon_r + 2\epsilon_{\text{rm}}} \vec{E}_0 = 4\pi R^3 \epsilon_0 \epsilon_{\text{rm}} \cdot \vec{E}_0 \quad (26)$$

Then the field enhancement factor at the poles is

$$F(\vec{r}_s) = \left| \vec{E}(\vec{r}_s) \right|^2 / \left| \vec{E}_0 \right|^2 = \lim_{\epsilon_r \rightarrow -\infty} \left( \frac{3\epsilon_r}{\epsilon_r + 2\epsilon_{\text{rm}}} \right)^2 = 9 \quad (27)$$

For the hot-spot between two adjacent metal spheres, the enhancement factor follows

$$F \approx \lim_{\epsilon_r \rightarrow -\infty} \left( \frac{5\epsilon_r - 2\epsilon_{\text{rm}}}{\epsilon_r + 2\epsilon_{\text{rm}}} \right)^2 = 25 \quad (28)$$

Therefore metal spheres also show the IDEE with the largest field enhancement factor regardless of the type of metal. However, the IDEE of metal spheres is distinguished from the surface plasmon enhancement

effect by the fact that no surface plasmon resonance is involved. It therefore works for a large wavelength range of light, in contrast to the surface plasmon enhancement effect which only exists within the range of resonance wavelengths. However, the surface plasmon enhancement effect can be much stronger than IDEE, because it occurs under the Fröhlich condition, i.e.,  $\text{Re}[\epsilon_r(\omega)] = -2\epsilon_{\text{rm}}$ , resulting in a huge enhancement factor because of the near zero denominators in Eqs. (27) and (28). In the scattering spectra, this resonance condition leads to a resonance peak. The surface plasmon enhancement effect is effective only when the incident light wavelength falls in this peak range. Outside this peak wavelength range, IDEE dominates the enhancement effect.

Considering that the peak of the localized surface plasmon resonance is relatively narrow compared with the Rayleigh spectral range, it is therefore not suitable for enhancing the Rayleigh scattering, because it will introduce extra spectral peaks in the Rayleigh spectra. However it is very suitable for enhancing Raman and fluorescence signals by properly selecting the excitation wavelength of laser in the resonance wavelength range.

In contrast, IDEE is widely applicable to enhance the Rayleigh, Raman, and fluorescence signals, but with moderate enhancement factors. IDEE is especially important for enhancing Rayleigh scattering, which further enables true-color real-time Rayleigh imaging of nanomaterials.

## 2.7 Near field of dipole lattices

For multiple dielectric spheres, it is usually not possible to obtain an analytical solution of the dipole field. We must rely on numerical calculations, such as the FDTD method. However, FDTD is usually very time consuming. Since we are only concerned about the dipole field, and the dielectric spheres can be represented by an equivalent dipole centered at the sphere, we can directly calculate the dipole field by summing up the field of each equivalent dipole.

Suppose the macroscopic light field is  $\vec{E}_0(t) = \vec{E}_0 e^{i\omega t}$  and  $\vec{E}_0(t)$  is polarized along the  $y$  direction, then the dipoles will oscillate in phase  $\vec{p}(t) = \vec{p} e^{i\omega t}$ . The

near field contributed by the  $i$ th dipole is  $\vec{E}_i(\vec{r}, t) = \frac{1}{4\pi\epsilon_0\epsilon_{\text{rm}}} \cdot \frac{3(\hat{r}_i \cdot \vec{p})\hat{r}_i - \vec{p}}{r_i^3} e^{i\omega t}$ . Again for the sake of convenience, the  $e^{i\omega t}$  term is omitted in the following text.

The near field contributed by all the dipoles is

$$\vec{E}_D = \sum_i \vec{E}_i = \frac{1}{4\pi\epsilon_0\epsilon_{\text{rm}}} \cdot \sum_i \frac{3(\hat{r}_i \cdot \vec{p})\hat{r}_i - \vec{p}}{r_i^3} \quad (29)$$

Since both  $\vec{E}_0$  and  $\vec{p}$  are in the  $y$  direction, only the  $y$ -component of  $\vec{E}_D$  needs to be calculated. Figure 3(a) shows the near field pattern of a 1-D dipole lattice with lattice constant  $a$ , assuming an induced dipole  $\vec{p}$  for each lattice point. Note that each lattice point may represent one atom, or one molecule, or one dielectric sphere with dimension much less than the wavelength of light. Apparently the dipole field is localized in the vicinity of the dipole lattice with some region enhanced and some region weakened.

First, let us look at the near field at positions  $(ma, a/2, 0)$  on the red dashed line shown in Fig. 3(a).

$$\vec{E}_{D+} = \beta_+ \cdot \frac{\vec{p}}{\epsilon_0\epsilon_{\text{rm}}a^3} \quad (30)$$

in which

$$\beta_+ = \frac{1}{4\pi} \sum_{n=-\infty}^{+\infty} \frac{2\left(n + \frac{1}{2}\right)^2 - m^2}{\left[\left(n + \frac{1}{2}\right)^2 + m^2\right]^{5/2}} \quad (31)$$

Numerical results are shown in Table 1 and Fig. 3(b). The key feature is that the dipole field decays very fast to zero within two lattice constants showing the near field nature. In addition, the positive value means the local field here is enhanced due to the near field of the dipoles.

Then we look at the near field at positions  $(ma, 0, 0)$  on the  $x$ -axis

$$\vec{E}_{D-} = \beta_- \cdot \frac{\vec{p}}{\epsilon_0\epsilon_{\text{rm}}a^3} \quad (32)$$

in which

$$\beta_- = \frac{1}{4\pi} \sum_{n=-\infty}^{+\infty} \frac{2n^2 - m^2}{(n^2 + m^2)^{5/2}} \quad (33)$$

Numerical results are also shown in Table 1 and Fig. 3(b). The near field also decays very fast to zero, but has a negative value, which means the local field here is weakened due to the near field of the dipoles. Here, both  $\beta_+$  and  $\beta_-$  are termed “dipole field factors”.

When SWCNTs are immersed in a liquid medium, such as water, the medium molecules tend to form clusters at the interface because of the interaction between the molecules and the carbon lattice, especially when the SWCNTs are charged [2]. The clusters are positioned at the centers of the hexagon and form a dielectric sphere lattice, as shown in Fig. 4(a). Our molecular dynamic simulations confirm the statistical average density distribution patterns of medium molecules for SWCNTs immersed in water and glycerol.

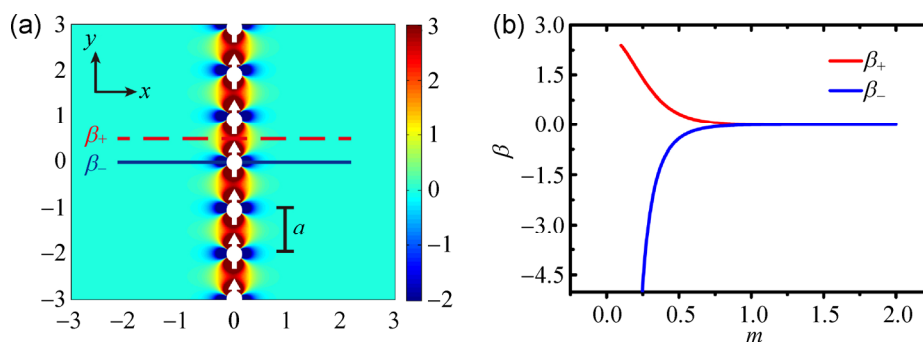


**Figure 3** 1-D dipole lattice model. (a) The position of the 1-D dipole lattice in the  $x$ - $y$  plane and the lattice constant of the 1-D dipole lattice is  $a$ . The calculated near field in the  $x$ - $y$  plane around the 1-D dipole lattice is also shown in the form of the color. (b) The dipole field factor  $\beta$  along the two lines shown in (a).  $m$  represents the distance to the 1-D dipole lattice along the  $x$  direction in the unit of lattice constant  $a$ .

**Table 1** The numerical results of the dipole field factor  $\beta$  at different distance

$m$	$\beta_+$	$\beta_-$	$m$	$\beta_+$	$\beta_-$
0.1	2.393	-79.205	0.7	0.087	-0.093
0.2	1.743	-9.602	0.8	0.044	-0.046
0.3	1.088	-2.641	0.9	0.022	-0.023
0.4	0.615	-0.982	1	0.011	-0.012
0.5	0.328	-0.421	1.5	3.9e-04	-4.2e-04
0.6	0.170	-0.194	2	-5.6e-07	-3.1e-05

Here we therefore calculate the dipole field factor  $\beta$  for dielectric sphere lattices on the surface of a SWCNT (Fig. 4(a)). Its dependence on the distance of the carbon atom to the lattice plane of the dielectric spheres is shown in Fig. 4(b), clearly showing the fast decaying feature of the dipole field. However, carbon atom will feel an enhanced near field if its distance to the lattice plane of dielectric spheres is less than one lattice constant.

**2.8 General formula for the field enhancement factor of dipole lattices**

To calculate the total field, first the relationship between  $\vec{E}_0$  and  $\vec{p}$  has to be determined. Consider that every dipole in the lattice will feel not only the excitation field  $\vec{E}_0$ , but also the dipole field contributed by all other dipoles termed  $\vec{E}_d$ . Therefore the local field felt by each dipole should be  $\vec{E}_{local} = \vec{E}_0 + \vec{E}_d$ , in which  $\vec{E}_d = \beta_0 \cdot \frac{\vec{p}}{\epsilon_0 \epsilon_{rm} a^3}$ .  $\beta_0$  is called the field factor at

the lattice point. Then the local field at each lattice point is

$$\vec{E}_{local} = \vec{E}_0 + \beta_0 \cdot \frac{\vec{p}}{\epsilon_0 \epsilon_{rm} a^3} \tag{34}$$

Note that this local field is locally uniform, just like the locally uniform field created by a Helmholtz coil, and the dielectric sphere will therefore behave like a huge dipole at the center. The relation between the induced dipole and the local field follows Eq. (20), which we copy here for convenience

$$\vec{p} = 4\pi R^3 \epsilon_0 \epsilon_{rm} \cdot \frac{\epsilon_r - \epsilon_{rm}}{\epsilon_r + 2\epsilon_{rm}} \vec{E}_{local} \tag{20'}$$

Combining Eqs. (34) and (20'), we have

$$\vec{p} = \frac{4\pi R^3 \epsilon_0 \epsilon_{rm} \cdot \frac{\epsilon_r - \epsilon_{rm}}{\epsilon_r + 2\epsilon_{rm}}}{1 - 4\pi \beta_0 \cdot \frac{R^3}{a^3} \cdot \frac{\epsilon_r - \epsilon_{rm}}{\epsilon_r + 2\epsilon_{rm}}} \vec{E}_0 \tag{35}$$

Then the total field should be

$$\vec{E} = \vec{E}_0 + \vec{E}_d = \vec{E}_0 + \beta \cdot \frac{\vec{p}}{\epsilon_0 \epsilon_{rm} a^3} = \left[ 1 + \frac{4\pi \beta \cdot \frac{R^3}{a^3} \cdot \frac{\epsilon_r - \epsilon_{rm}}{\epsilon_r + 2\epsilon_{rm}}}{1 - 4\pi \beta_0 \cdot \frac{R^3}{a^3} \cdot \frac{\epsilon_r - \epsilon_{rm}}{\epsilon_r + 2\epsilon_{rm}}} \right] \vec{E}_0 \tag{36}$$

and the general formula for the field enhancement factor reads

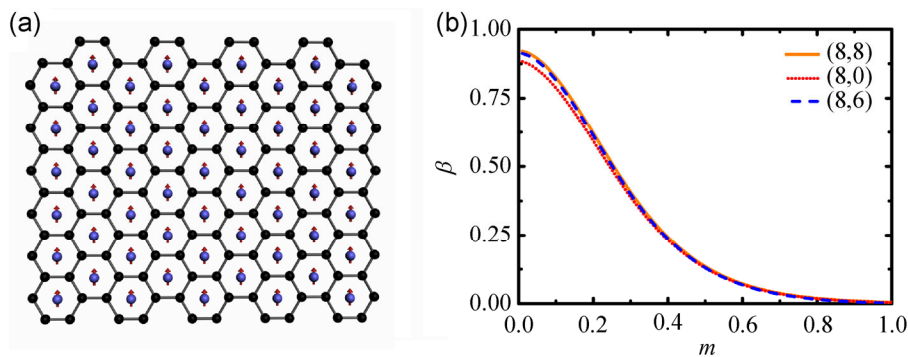


**Figure 4** Lattice of optical dipoles on the surface of single-walled carbon nanotubes and the dipole field factor for single-walled carbon nanotubes with different chirality indices. (a) Schematic illustration of the distribution of dielectric spheres and crystal lattices of SWCNT. (b) The relationship between the field factor  $\beta$  to the distance  $m$  for SWCNTs with different chiral indices.  $m$  represents the distance of the carbon atom to the lattice plane of the dielectric spheres.

$$F = \left| \bar{E} \right|^2 / \left| \bar{E}_0 \right|^2 = \left[ 1 + \frac{4\pi\beta \cdot \frac{R^3}{a^3} \cdot \frac{\epsilon_r - \epsilon_{rm}}{\epsilon_r + 2\epsilon_{rm}}}{1 - 4\pi\beta_0 \cdot \frac{R^3}{a^3} \cdot \frac{\epsilon_r - \epsilon_{rm}}{\epsilon_r + 2\epsilon_{rm}}} \right]^2 \quad (37)$$

In the case of  $a \approx 2R$ , and in most lattices  $\pi\beta_0 \approx 1$ , Eq. (37) has a very simple form

$$F = \left| \bar{E} \right|^2 / \left| \bar{E}_0 \right|^2 \approx \left[ 1 + \pi\beta \frac{\epsilon_r - \epsilon_{rm}}{\epsilon_r + 5\epsilon_{rm}} \right]^2 = \left[ 1 + \pi\beta \left( 1 - \frac{6}{\frac{\epsilon_r}{\epsilon_{rm}} + 5} \right) \right]^2 \quad (37')$$

It is clear that a larger  $\beta$  and  $\frac{\epsilon_r}{\epsilon_{rm}}$  will give rise to a larger field enhancement factor. Here we would like to stress that  $\epsilon_r$  is the dielectric constant of the interfacial material, which is much larger than the dielectric constant of the corresponding bulk material (see Section 3.2).

### 3 IDEE and enhanced Rayleigh scattering

Rayleigh scattering is the elastic scattering of light by particles or small volumes of density fluctuation which are much smaller than the wavelength of light, and it is well known as the cause of the blue sky [5]. In the case of nanomaterials such as SWCNTs, typical Rayleigh scattering spectra show resonance peaks due to the optically allowed interband transitions [11, 12]. Though excitonic in nature [13–15], the resonance peaks are related to the van Hove singularities (vHS) in the electron density of states, thus enable chirality assignment of SWCNTs [16–20].

Recently we discovered that Rayleigh scattering of SWCNTs can be greatly enhanced by an interfacial layer of high refractive index materials, which has enabled true-color real-time imaging and spectroscopy of SWCNTs for high throughput chirality assignment [3]. This finding has led to an intense theoretical investigation, and as a result, IDEE has been proposed to explain it. The most straightforward and decisive evidence supporting IDEE is that dim SWCNTs on a quartz substrate become bright and show chirality dependent color after being covered by a wetting

layer of glycerol [3]. Here we show more experimental evidence in support of IDEE.

#### 3.1 General considerations of enhanced Rayleigh scattering

The Rayleigh scattering of SWCNTs is weak due to the small cross section of Rayleigh scattering. To realize Rayleigh scattering imaging or spectroscopy, some enhancement methods for Rayleigh scattering of SWCNTs must be employed.

The most straightforward method is to increase the intensity of the incident light. This method works well with suspended SWCNTs, but is limited by the heating effect which will lead to burning of SWCNTs in air. However, for SWCNTs on substrates, this method does not work, because the Rayleigh scattering of the substrate is simultaneously enhanced, and the contrast of Rayleigh imaging of SWCNTs cannot be improved.

Another method is to enhance the boundary field and simultaneously diminish the substrate scattering simply by immersing the samples in water [3]. Compared with samples in air, the samples in water feel an enhanced boundary field resulting in enhanced Rayleigh scattering. At the same time, the substrate scattering is greatly reduced leading to a better contrast of the Rayleigh image.

If water is replaced by glycerol, the substrate scattering is almost totally removed because of the better refractive index matching. The field felt by SWCNTs is further enhanced compared with that in water. The nearly perfect refractive index matching makes SWCNTs on substrates act like SWCNTs suspended in a liquid. However, there is also a problem of severe Rayleigh scattering from the density fluctuation of liquids when the incident light intensity is increased.

An ideal method is to locally enhance the Rayleigh scattering of SWCNTs without enhancing the Rayleigh scattering of the substrate or surrounding medium, which is the recently proposed interface dipole enhanced Rayleigh scattering (IDERS) method [3]. The key point of this method is to introduce a high refractive index interfacial layer between the medium and SWCNTs, which will provide an additional near field acting on the SWCNTs and thus enhance the Rayleigh scattering.

However, this high refractive index interfacial layer will also scatter light which may hinder Rayleigh imaging of SWCNTs. Therefore there are some requirements for IDERS as below: (1) The interfacial layer of condensed molecules must be thin enough to guarantee that the Rayleigh scattering from this layer is weaker than that from the sample; (2) there are no characteristic peaks from the interfacial molecules in the visible region. Fortunately all the requirements can be fulfilled using the medium of water or glycerol in this study.

### 3.2 Implementation of interface dipole enhanced Rayleigh scattering

The first implementation of interface dipole enhancement Rayleigh scattering (IDERS) is realized by immersing the samples in water and a water immersion objective is used to collect the Rayleigh scattered light. Schematic illustrations of the Rayleigh imaging microscopy are shown in Figs. 5(a) and 5(b), corresponding to the schemes using oblique light excitation and evanescent wave excitation respectively. A typical Rayleigh image of SWCNTs on quartz substrate is shown in Fig. 5(c). Here water plays several roles, such as enhancing the boundary field, and diminishing substrate scattering by refractive index matching [3].

Most importantly, a high density shell of water molecules is naturally formed around SWCNT according to molecular dynamics (MD) simulations (Fig. 5(d)).

The Clausius–Mossotti relation [7]  $\epsilon_r - 1 = \frac{N\alpha}{1 - (N\alpha/3)}$

tells us that higher density of  $N$  at the interfacial layer than that in bulk region (Fig. 5(e)) implies a higher dielectric constant and higher refractive index. This high refractive index shell of water molecules gives rise to larger  $\frac{\epsilon_r}{\epsilon_{rm}}$  and will enhance the Rayleigh

scattering of SWCNT according to our IDEE theory (see Eq. (37')), which enables true-color real-time Rayleigh imaging of SWCNTs.

In the second implementation of IDERS, the samples are immersed in glycerol and an oil immersion objective is used to collect the Rayleigh scattered light. The excitation light path is schematically illustrated in Fig. 6(a). A typical Rayleigh image of SWCNTs on a quartz substrate is shown in Fig. 6(b). Compared with water, the refractive index of glycerol is closer to that of quartz, leading to an ideal refractive index matching condition. Consequently the substrate scattering is eliminated and the excitation light field is further enhanced compared with that in water. Similar to water, a high density layer of glycerol

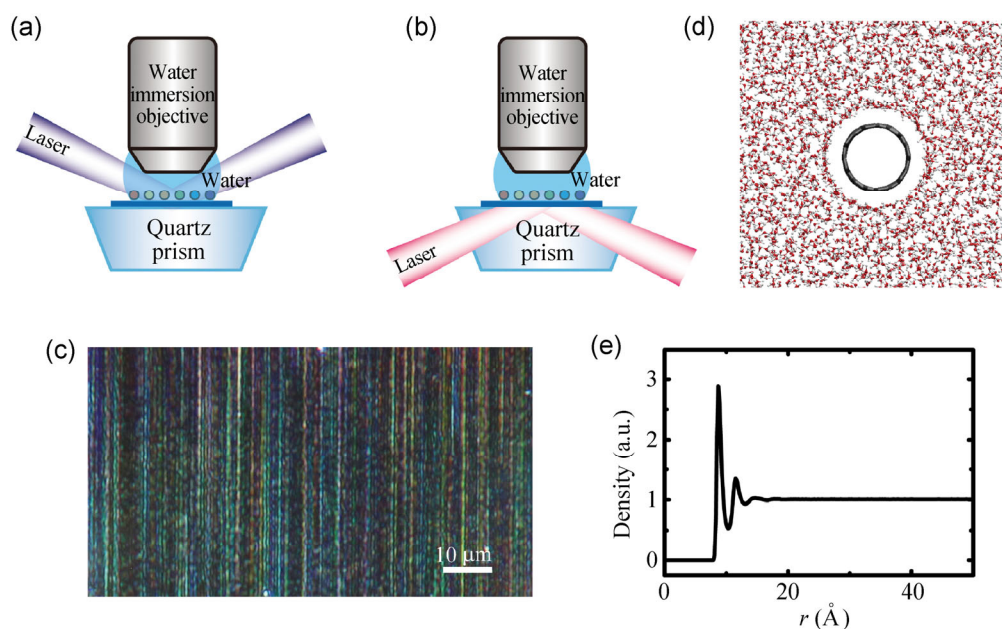


**Figure 5** True-color real-time imaging and molecular dynamics simulation of SWCNTs immersed in water. (a) and (b) Two kinds of illumination setups for SWCNTs on quartz immersed in water. (c) A typical true-color image of SWCNTs immersed in water. (d) Cross sectional view of an individual (8, 8) SWCNT in water simulated by molecular dynamics. (e) The number density of water molecule along the radial direction and the axis of the SWCNT is set at zero.

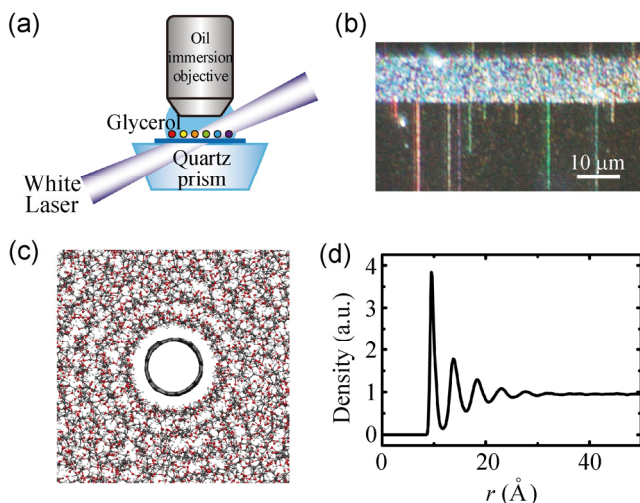


**Figure 6** True-color real-time imaging and molecular dynamics simulation of SWCNTs immersed in glycerol. (a) Illumination setup for SWCNTs on quartz immersed in glycerol. (b) A typical true-color image of SWCNTs immersed in glycerol. (c) Cross sectional view of an individual (8, 8) SWCNT in glycerol simulated by molecular dynamics. (d) The number density of glycerol molecule along the radial direction and the axis of the SWCNT is set at zero.

molecules is also naturally formed around SWCNT (Fig. 6(c)). However, the density increase of glycerol is greater than that for water, which leads to larger  $\frac{\epsilon_r}{\epsilon_m}$ , as well as larger field enhancement factor. This is the reason why the Rayleigh image in glycerol is more distinct than that in water. Before this work, Joh and colleagues achieved false-color Rayleigh imaging of SWCNTs immersed in glycerol [17], but they did not realize that glycerol helps enhanced Rayleigh scattering by IDEE.

The first two implementations utilize only one medium, but involves different densities at the interface and bulk, which gives rise to large  $\frac{\epsilon_r}{\epsilon_m}$  and large field enhancement factor, to achieve the IDERS. However, it is also possible to introduce another medium at the interface to generate a large  $\frac{\epsilon_r}{\epsilon_m}$  and a large enhancement factor. The following two implementations use this principle to achieve IDERS.

The third implementation involves another dielectric material at the interface between SWCNTs and water. Before putting the samples into a water prism, a droplet of alcohol or isopropanol is dropped onto the

surface of the sample. An interfacial layer of alcohol or isopropanol will naturally form on the surface of SWCNTs because of wetting. This heterogeneous interfacial layer also gives rise to IDERS. Note that this layer of alcohol or isopropanol has another function of avoiding electrolysis of water when SWCNTs are charged. Another example is when SWCNTs are transferred from a quartz substrate to a silicon wafer using PMMA. The residual PMMA on the surface of SWCNTs serves as a high refractive index interfacial layer when immersed in water, and gives rise to a huge enhancement factor to achieve IDERS [3]. Details can be found in Ref. [3]. Here we would like to suggest that this heterogeneous interfacial layer should also have a different density, as well as different dielectric constant from bulk materials. Furthermore, the term

$\frac{\epsilon_r}{\epsilon_m}$  in Eq. (37') reminds us that smaller  $\epsilon_m$  will give rise to a larger enhancement factor. Thus when the same interfacial material is used and the sample is placed in air rather than in water, the enhancement factor will be further improved, which has been shown by our experimental results [3]. The Rayleigh scattering from SWCNT is so strong that the substrate scattering is no longer noticeable.

The last implementation is to use nanometer sized metal particles. As we discussed in Section 2.6, in the wavelength range away from surface plasmon resonance, the metal particles also behave as interface dipoles leading to stronger IDEE than dielectric spheres. The drawback is that they will introduce an extra spectral peak due to the surface plasmon resonance in the Rayleigh scattering spectra. However, they are very helpful for Rayleigh imaging microscopy because of their large enhancement effect. Figures 7(a) and 7(b) show the Rayleigh imaging of SWCNTs due to the IDEE contributed by gold nanoparticles. The Rayleigh scattering of SWCNTs is clearly enhanced giving rise to a more distinct Rayleigh image. At the same time, the yellowish color due to the surface plasmon resonance can also be directly noticed, as expected.

### 3.3 Charge effect

According to Eq. (37'), our IDEE theory predicts that

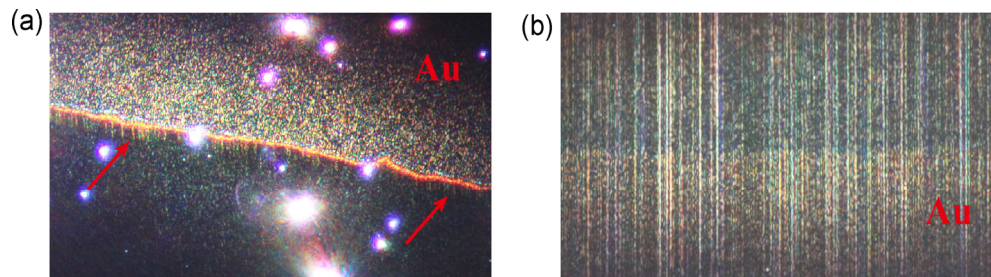


**Figure 7** Enhanced Rayleigh scattering by metal nanoparticles. (a) When Au electrodes about 50 nm thick are deposited on the quartz by a shadow mask, some of the SWCNTs around the edge is also covered by some tiny Au nanoparticles. The Rayleigh scattering of some SWCNTs with Au nanoparticles is greatly enhanced and some of them show chirality dependent color. (b) The SWCNTs at the bottom part was deposited with nominal 2 nm Au using a shadow mask. Due to the interface dipole enhancement by the Au nanoparticles, the Rayleigh scattering of SWCNTs at the lower part was enhanced compared with the ones at the upper part under the same illumination.

larger  $\beta$  and  $\frac{\epsilon_r}{\epsilon_{rm}}$  will give rise to a larger field enhancement factor. In addition  $\beta$  is very sensitive to the distance between SWCNT and dipole lattices. Smaller distances will lead to a larger  $\beta$  and a larger field enhancement factor. MD simulations show that, if SWCNT is negatively charged either in water or glycerol (Fig. 8), the density increase of the interfacial layer becomes more marked while the distance between the interfacial layer and SWCNT becomes

smaller. The density increase will lead to larger  $\frac{\epsilon_r}{\epsilon_{rm}}$ , and the smaller distance will result in a larger  $\beta$ , therefore a larger field enhancement factor is expected for charged SWCNTs according to our IDEE theory.

To verify this prediction, an experiment involving *in situ* Rayleigh imaging of the gradually charged SWCNT in glycerol was designed and conducted. To inject electrons into the SWCNTs, electrodes were patterned on the quartz substrates. Figure 9 shows

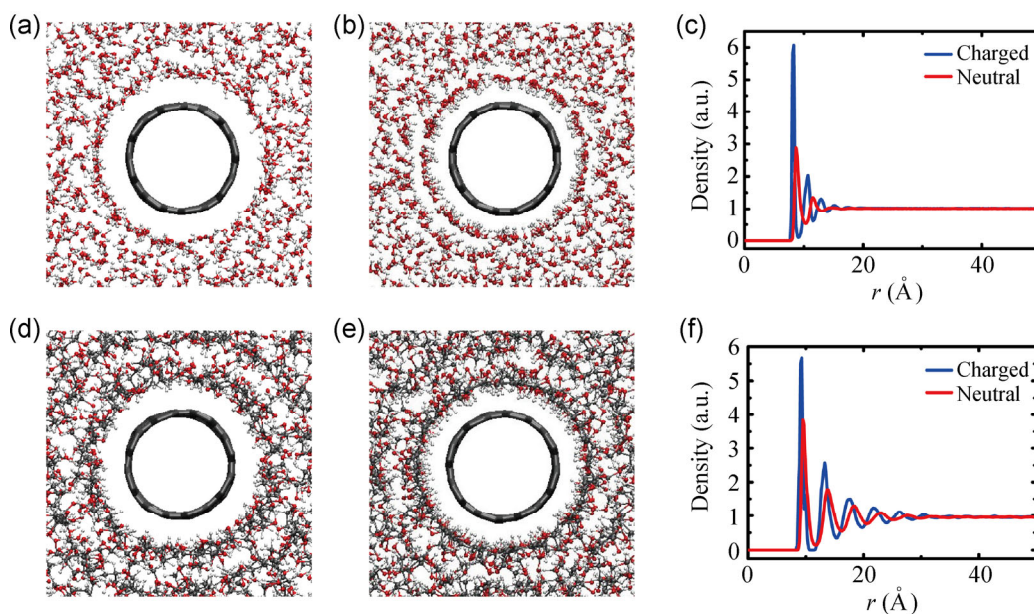


**Figure 8** Molecular dynamics simulations of neutral and negative charged single-walled carbon nanotubes immersed in water and glycerol. Cross sectional views of (a) neutral and (b) negative charged SWCNTs immersed in water. (c) The number density of water molecule around the neutral and negative charged SWCNT along the radial direction and the axis of the SWCNT is set at zero. Cross sectional views of (d) neutral and (e) negative charged SWCNTs immersed in glycerol. (f) The number density of glycerol molecule around the neutral and negatively charged SWCNT along the radial direction with the axis of the SWCNT set at zero.

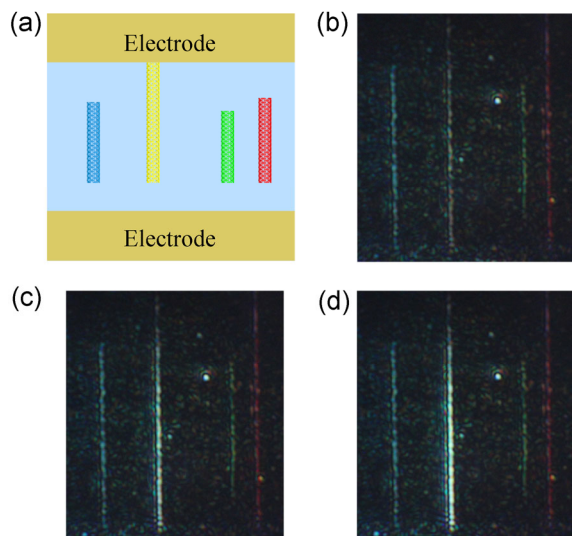


**Figure 9** Charge effect on the Rayleigh scattering of SWCNTs immersed in glycerol. (a) Schematic illustration of the positions of SWCNTs on quartz and electrodes. (b)–(d) Rayleigh images of SWCNTs during the charge process. (b)–(d) are among the series of images and show that the Rayleigh scattering of SWCNTs is greatly enhanced when the SWCNT is charged.

four SWCNTs, of which only the yellow one is connected to the upper electrode and the other three are connected to neither electrode. When a negative voltage ( $-2\text{ V}$ ) is applied to the upper electrode and the lower grounded, only the yellow SWCNT is charged. As time went on, the Rayleigh scattering of the yellow SWCNT was greatly enhanced while the remaining SWCNTs were unchanged. Furthermore, the enhancement of the Rayleigh scattering became weak again after the SWCNTs were discharged. Here we would like to stress that this enhancement effect is not due to the electron doping of SWCNTs, because there is no enhancement effect observed for either electron or hole doped SWCNTs in air [20]. Thus, the enhanced Rayleigh scattering of SWCNTs observed here supports the IDEE theory.

The *in situ* spectra of an individual SWCNT during the charge process were also recorded as illustrated in Fig. 10. The black line represents the Rayleigh scattering of a neutral SWCNT and the other three lines are the enhanced Rayleigh scattering spectra during the charge process. It is obvious that the scattering intensity is enhanced while the shape and position of the resonance peaks remain the same.

All the above experimental results are consistent with the predictions of our IDEE theory.

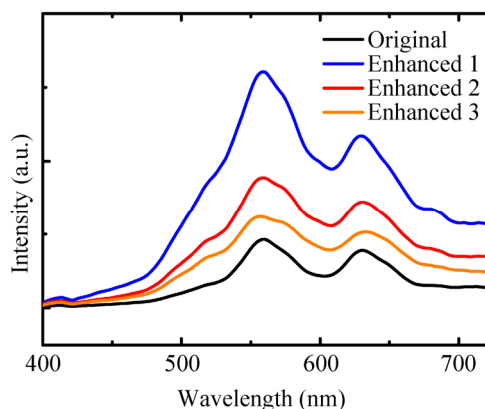


**Figure 10** Rayleigh spectra of an individual SWCNT immersed in glycerol. The black line is the spectrum of the SWCNT before it is charged. The other three lines are the spectra of the SWCNT during the charge process.

## 4 Conclusions

The interface dipole enhancement effect has been systematically described theoretically and verified by experiments. The near field of the interfacial optical dipoles is vital for nanomaterials, which can be treated in a microscopic picture under the condition of the static field approximation. As a result of the secondary radiation of the optical dipoles, the light field is distorted and the field in some regions is greatly enhanced, which provides a method to locally enhance the excitation field of the nanomaterials. By means of IDEE, the Rayleigh scattering of SWCNTs can be greatly enhanced by the interface dipoles, which helps true-color real-time imaging of SWCNTs. Furthermore, IDEE is a widespread effect for nanomaterials, and can be taken advantage of to study interface-related phenomenon.

However, IDEE is not restricted to enhancing Rayleigh scattering. It might also lead to interface dipole enhanced Raman spectra and interface dipole enhanced fluorescence of atoms, molecules, and nanomaterials, which needs further extensive investigations.

## 5 Methods

### 5.1 Rayleigh imaging microscopy and spectroscopy of SWCNTs

Figures 5(a), 5(b), and 6(a) show simplified schematic

illustrations of our experimental setups for true-color real-time imaging of nanomaterials. A supercontinuum white laser (Fianium SC400) is used as the oblique illuminating light source, and a standard optical microscope is used to collect the Rayleigh scattered light. In the experimental setup shown in Figs. 5(a) and 5(b), a water immersion objective (Leica L 63×/0.9) is used to view the samples immersed in water. In the experimental setup shown in Fig. 6(a), an oil immersion objective (OLYMPUS UPlanFLN 100×/1.30) is used to view the samples immersed in glycerol. A general purpose digital camera with low cost CMOS image sensor (Canon EOS600D) is adopted to conveniently record the images and real-time video. A detailed illustration of the Rayleigh imaging microscope can be found in Ref. [3]. Combining the Rayleigh imaging microscope with a spectrometer, Rayleigh imaging assisted spectroscopy can be used to record the Rayleigh scattering spectra of individual SWCNTs, as is shown in Ref. [3].

## 5.2 Molecular dynamics (MD) simulations related to SWCNT

We carried out two molecular dynamics (MD) simulations of an infinitely long, hollow CNT in glycerol and water as solvents. The CNT in our simulations is an (8, 8) armchair type, with a C–C diameter of  $\sim 10.5$  Å. The CNT is periodic along its axis (aligned with the  $z$ -axis) with a unit length of  $\sim 34$  Å. The CNT was then solvated in 3,404 glycerol molecules or 15,086 water molecules, resulting in a total of 48,104 or 45,706 atoms in the two systems, respectively. The interior of the CNT was empty of any solvent.

To facilitate equilibration, we performed a simulated annealing of 2 ns for each of the systems, in which the temperature was gradually reduced from 500 to 300 K, as controlled by the Langevin dynamics method. This equilibration was then followed by a production run of 50 ns at a constant temperature of 300 K for each system, and the last 40 ns of the simulation trajectory was used for analysis. All atoms (including the CNT atoms) were free to move in these simulations.

Simulation parameters for carbon atoms of the

CNT were those of type “CA” for aromatic carbon in the CHARMM protein force field [21]. All CNT atoms were assigned zero charge. The parameters for glycerol were taken from the CHARMM carbohydrate force field [22]. The TIP3P water model [23] was adopted in the CNT–water simulations. All simulations were performed using the NAMD2 (Ver. 2.9) program [24] with a time step of 2 fs. All bond lengths involving hydrogen atoms were constrained using the SHAKE [25] and SETTLE [26] algorithms. We adopted a cutoff distance of 12 Å for nonbonded interactions, with a smooth switching function taking effect at 10 Å. Full electrostatics was calculated every 4 fs using the particle-mesh Ewald method [27]. A constant pressure of 1 atm was achieved using the Nose–Hoover Langevin piston method [28], with the size of the periodic box allowed to fluctuate but the ratio in the  $x$ – $y$  plane kept fixed to 1. During our simulations the lengths of the periodic box were stabilized at  $\sim 113$  Å  $\times$  113 Å  $\times$  34 Å and  $\sim 115$  Å  $\times$  115 Å  $\times$  34 Å for the glycerol and water systems, respectively.

## Acknowledgements

The authors thank Prof. Wei Zhang, Prof. Yidong Huang, Dr. Li Fan, and Prof. Ping Xue for their kind help. This work was supported by the National Basic Research Program of China (No. 2012CB932301) and the National Natural Science Foundation of China (Nos. 90921012, 11321091, 51102144, 11274190, and 51102147).

## List of symbols

$\vec{E}$	electric field
$\vec{E}_0$	incident light field
$\vec{p}_0$	optical dipole of an atom
$\alpha$	atomic polarizability
$\epsilon_0$	permittivity of the vacuum
$\vec{E}_{\text{local}}$	local field at the position of an atom
$\phi_D$	electric potential of a dielectric sphere
$\vec{P}$	mean dipole moment density
$M$	total number of optical dipoles inside a dielectric sphere
$V$	volume of a dielectric sphere

$\bar{p}$	equivalent dipole moment of a dielectric sphere
$\bar{E}_D$	secondary radiation field of dipoles
$N$	number density of the atoms in a dielectric sphere
$F$	field enhancement factor
$\epsilon_r$	dielectric constant
$\beta$	dipole field factor
$a$	lattice constant of the dipole chain
$m$	distance factor for the distance from the SWCNTs to dipole lattices
$\bar{E}_d$	dipole field contributed by dipole lattices
$n$	refractive index

## References

- Walther, J. H.; Jaffe, R.; Halicioglu, T.; Koumoutsakos, P. Carbon nanotubes in water: Structural characteristics and energetics. *J. Phys. Chem. B.* **2001**, *105*, 9980–9987.
- Huang, B. D.; Xia, Y. Y.; Zhao, M. W.; Li, F.; Liu, X. D.; Ji, Y. J.; Song, C. Distribution patterns and controllable transport of water inside and outside charged single-walled carbon nanotubes. *J. Chem. Phys.* **2005**, *122*, 0847088.
- Wu, W. Y.; Yue, J. Y.; Lin, X. Y.; Li, D. Q.; Zhu, F. Q.; Yin, X.; Zhu, J.; Wang, J. T.; Zhang, J.; Chen, Y.; et al. True-color real-time imaging and spectroscopy of carbon nanotubes on substrates by enhanced Rayleigh scattering. **2014**, submitted.
- Ashcroft, N. W.; Mermin, N. D. *Solid State Physics*; Saunders College: New York, 1976.
- Fabelinskii, I. L. *Molecular Scattering of Light*; Plenum Press: New York, 1968.
- Sargent III, M.; Scully, M. O.; Lamb Jr, W. E. *Laser Physics*; Addison Wesley: New York, 1974.
- Feynman, R. P.; Leighton, R. B.; Sands, M. *The Feynman Lectures on Physics, Mainly Electromagnetism and Matter, Volume II*; Addison-Wesley: Reading, Massachusetts, 1977.
- Kittel, C. *Introduction to Solid State Physics (8th edition)*; Wiley: New York, 2004.
- Jackson, J. D. *Classical Electrodynamics (3rd edition)*; Wiley: New York, 1998.
- Maier, S. A. *Plasmonics: Fundamentals and Applications*; Springer: New York, 2007.
- Yu, Z.; Brus, L. Rayleigh and Raman scattering from individual carbon nanotube bundles. *J. Phys. Chem. B.* **2001**, *105*, 1123–1134.
- Sfeir, M. Y.; Wang, F.; Huang, L. M.; Chuang, C. C.; Hone, J.; O'Brien, S. P.; Heinz, T. F.; Brus, L. E. Probing electronic transitions in individual carbon nanotubes by Rayleigh scattering. *Science* **2004**, *306*, 1540–1543.
- Dresselhaus, M. S.; Dresselhaus, G.; Saito, R.; Jorio, A. Exciton photophysics of carbon nanotubes. *Annu. Rev. Phys. Chem.* **2007**, *58*, 719–747.
- Berciaud, S.; Voisin, C.; Yan, H. G.; Chandra, B.; Caldwell, R.; Shan, Y. Y.; Brus, L. E.; Hone, J.; Heinz, T. F. Excitons and high-order optical transitions in individual carbon nanotubes: A Rayleigh scattering spectroscopy study. *Phys. Rev. B.* **2010**, *81*, 041414.
- Joh, D. Y.; Kinder, J.; Herman, L. H.; Ju, S. Y.; Segal, M. A.; Johnson, J. N.; ChanGarnet, K. L.; Park, J. Single-walled carbon nanotubes as excitonic optical wires. *Nat. Nanotech.* **2011**, *6*, 51–56.
- Sfeir, M. Y.; Beetz, T.; Wang, F.; Huang, L. M.; Huang, X. M. H.; Huang, M. Y.; Hone, J.; O'Brien, S.; Misewich, J. A.; Heinz, T. F.; et al. Optical spectroscopy of individual single-walled carbon nanotubes of defined chiral structure. *Science* **2006**, *312*, 554–556.
- Joh, D. Y.; Herman, L. H.; Ju, S. Y.; Kinder, J.; Segal, M. A.; Johnson, J. N.; Chan, G. K. L.; Park, J. On-chip Rayleigh imaging and spectroscopy of carbon nanotubes. *Nano Lett.* **2011**, *11*, 1–7.
- Lefebvre, J.; Finnie, P. Polarized light microscopy and spectroscopy of individual single-walled carbon nanotubes. *Nano Res.* **2011**, *4*, 788–794.
- Liu, K. H.; Deslippe, J.; Xiao, F. J.; Capaz, R. B.; Hong, X. P.; Aloni, S.; Zettl, A.; Wang, W. L.; Bai, X. D.; Louie, S. G.; et al. An atlas of carbon nanotube optical transitions. *Nat. Nanotech.* **2012**, *7*, 325–329.
- Liu, K. H.; Hong, X. P.; Zhou, Q.; Jin, C. H.; Li, J. H.; Zhou, W. W.; Liu, J.; Wang, E. G.; Zettl, A.; Wang, F. High-throughput optical imaging and spectroscopy of individual carbon nanotubes in devices. *Nat. Nanotech.* **2013**, *8*, 917–922.
- MacKerell, A. D.; Bashford, D.; Bellott, M.; Dunbrack, R. L.; Evanseck, J. D.; Field, M. J.; Fischer, S.; Gao, J.; Guo, H.; Ha, S.; et al. All-atom empirical potential for molecular modeling and dynamics studies of proteins. *J. Phys. Chem. B.* **1998**, *102*, 3586–3616.
- Hatcher, E. R.; Guvench, O.; MacKerell Jr, A. D. CHARMM additive all-atom force field for acyclic polyalcohols, acyclic carbohydrates, and inositol. *J. Chem. Theory Comput.* **2009**, *5*, 1315–1327.
- Jorgensen, W. L.; Chandrasekhar, J.; Madura, J. D.; Impey, R. W.; Klein, M. L. Comparison of simple potential functions for simulating liquid water. *J. Chem. Phys.* **1983**, *79*, 926–935.
- Phillips, J. C.; Braun, R.; Wang, W.; Gumbart, J.; Tajkhorshid, E.; Villa, E.; Chipot, C.; Skeel, R. D.; Kalé, L.;

- Schulten, K. Scalable molecular dynamics with NAMD. *J. Comput. Chem.* **2005**, *26*, 1781–1802.
- [25] Ryckaert, J-P.; Ciccotti, G.; Berendsen, H. J. Numerical integration of the cartesian equations of motion of a system with constraints: Molecular dynamics of *n*-alkanes. *J. Comput. Phys.* **1977**, *23*, 327–341.
- [26] Miyamoto, S.; Kollman, P. A. SETTLE: An analytical version of the SHAKE and RATTLE algorithm for rigid water models. *J. Comput. Chem.* **1992**, *13*, 952–962.
- [27] Darden, T.; York, D.; Pedersen, L. Particle mesh Ewald: An *N*·log(*N*) method for Ewald sums in large systems. *J. Chem. Phys.* **1993**, *98*, 10089–10092.
- [28] Feller, S. E.; Zhang, Y.; Pastor, R. W.; Brooks, B. R. Constant pressure molecular dynamics simulation: The Langevin piston method. *J. Chem. Phys.* **1995**, *103*, 4613–4621.